Double-Layered Droop Control-Based Frequency Restoration and Seamless Reconnection of Isolated Neighboring Microgrids for Power Sharing

Sandipan Patra, *Member, IEEE*, and Malabika Basu, *Member, IEEE*

***Abstract*— This article describes a seamless reconnection topology for power sharing between distant rural community microgrids (CMGs), which is based on a double-layered droop-controlled (DLDC) frequency restoration scheme. Increased load demand, along with the intermittent nature of renewable energy sources, may result in a power deficit in isolated CMGs. In order to overcome this restriction, the connection of autonomous neighboring CMGs may be a viable alternative to intelligent load shedding. When dealing with active power fluctuation and setting a frequency set point becomes difficult in the absence of a grid frequency reference, this DLDC-based approach can resolve the issue. The DLDC adds a self-synchronized feature by parallel shifting of the $f-P$ slope to restore the operating frequency to its nominal value. The difference in frequency enables to shift the voltage axis accordingly through the change in V_d and V_q reference of the terminal voltage for appropriate power sharing. The stability of the proposed controller has been analyzed by using a mathematical model considering communication delay in the distributed secondary controller. Finally, the efficacy of the proposed controller is shown via the use of unique processor-in-the-loop (PIL) experimental findings, in which OPAL-RT and PLECS RT boxes are used to build both the CMGs and a TI-based F28069M microprocessor is utilized as a controller.**

***Index Terms*— Community microgrid (CMG), droop control, frequency restoration, grid forming inverter, isolated microgrid.**

I. Introduction

In a rural area where large grid power is not available, the small-scale autonomous MGs can be economical to meet the local load demand. These community-based MGs are typically formed in a way to generate enough power to supply the local load demand. However, due to the sporadic nature of renewable energy sources and the uncertainty in load demand can create an energy deficiency, which can further generate a voltage/frequency drop in the system. To overcome this concern, an intelligent load shedding/demand response technique [1], [2] can be adopted. The alternative option is to install micro storage (MS) devices such as battery energy storage systems (BESS), flywheels, and diesel generators [3], but may not be economical in small-scale installation. However, a central storage device can be installed for a particular community-based MG. In this respect, the coupling of neighboring isolated community microgrids (CMGs) is technically and economically more viable for power sharing in case of any energy deficiency [4], [5], [6].

The CMG is usually connected with the neighboring one through an interfacing inverter. If the CMGs are not pre-synchronized, a significant inrush current can pose a major hazard to the entire system. On the other hand, the CMGs should be decoupled in order to ensure system stability in the event of any malfunction/emergency. The development of a smooth connection/recommission topology is thus crucial for the efficient operation of power sharing among adjacent CMGs.

The frequency, voltage, and phase angle of both the interface inverters must be identical for a smooth reconnection between contiguous CMG. Additional difficulties include maintaining power-sharing precision and system frequency, especially for the isolated CMGs. The most frequently utilized $Q-V$ and $P-f$ droop control is used for active and reactive power sharing between the MGs. In conventional droop control after attaining the power-sharing accuracy, the frequency may not necessarily maintain the nominal value. As a result, an additional control technique is required to restore the frequency and voltage of the CMGs. Thus, a seamless reconnection topology with a frequency restoration feature has to be developed to couple the neighboring CMGs for available power sharing.

The seamless reconnection and frequency restoration of isolated neighboring CMGs are a relatively new issue as all the regulatory authorities recently started to promote the development of renewable energy-based rural, isolated energy communities [7], [8]. However, much research [9] has been conducted for seamless transfer of operation modes between conventional grid and islanded microgrid. A linear integration method [10], phase angle synchronization [11], and virtual impedance-based (synchronverter [12], [13]) reconnection already proposed for the seamless transfer of modes. Most of these methods are based on phase-locked loops (PLLs), which have a built-in restriction on how local loads may be connected. To properly deploy these topologies, the local load must be decoupled during pre-synchronization.

Manuscript received 2 November 2021; revised 17 March 2022, 14 May 2022, and 3 July 2022; accepted 6 August 2022. Date of publication 10 August 2022; date of current version 3 October 2022. Recommended for publication by Associate Editor Yilmaz Sozer. *(Corresponding author: Malabika Basu.)*

The authors are with the School of Electrical and Electronic Engineering, TU Dublin, Dublin D07 EWV4, Ireland (e-mail: malabika.basu@TUDublin.ie).

Color versions of one or more figures in this article are available at https://doi.org/10.1109/JESTPE.2022.3197729.

Digital Object Identifier 10.1109/JESTPE.2022.3197729

The seamless mode transfer based on droop control was proposed in [14]. Again, the use of PLLs, which are intrinsically nonlinear, decreases substantially the reaction time and accuracy of power sharing. In an isolated rural microgrid where the R/X ratio is very high (with a ratio of $R/X > 5.5$), the conventional droop control interrelates a cross-coupling between $Q–V$ and $P–f$ droop control, which have a drastic effect on the power-sharing performance [15]. Conventionally, virtual impedance or virtual damping-based controller [16], [17] is introduced by the researchers in order to resolve this issue. Sometimes, this results in a significant voltage drop from its nominal value. The voltage drop over the high resistive rural coupling network can cause an inaccurate reactive power sharing that can introduce a circulating current among the coupled MGs [18]. In order to improve the active power-sharing performance of the droop controller in a highly resistive networked microgrid, a very high droop gain is required, which leads to a significant frequency/voltage drop in the system [19]. However, frequency management is crucial for smooth reconnection in inertialess isolated microgrids. Eventually, a secondary controller is introduced by the microgrid central controller (MGCC) to restore the frequency to its nominal value. All the recently proposed frequency restoration methods can be divided into three main categories—centralized, decentralized, and consensus control topologies [20], [21], [22], [23]. The communication channel-based secondary controller usually suffers from a single-point-of-failure, and the extra computational burden (due to massive data handling) can lead to poor dynamic performance [24]. Adaptive droop controller [25], virtual impedance-based adaptive droop controller [26], and optimized adaptive droop controller [27] can provide an accurate active power-sharing performance, faster dynamic response, and a significant stability margin to the system. However, the performance deviates in the presence of low impedance network and with critical loads (such as constant power loads). It is difficult to choose the suitable coefficient for the integral-derivative term and droop filter gain, which imposes power quality problems to the system. The signal injection-based frequency/voltage restoration method [16], [28] has been recently introduced by the researchers, which estimates the MG frequency/voltage based on the injected signal. If the estimated voltage/frequency deviates from its nominal value, then the MGCC adjusts the droop gain, in order to restore the nominal value. Due to the insertion of a signal, these techniques may result in poor power quality in the system.

Most of the proposed control methods as discussed above for frequency regulation/restoration are for a single unit of the microgeneration system. These researchers are mainly focused on the negative effect of low inertia on inadequate dynamic response following significant disturbances when the transient frequency dip can become unacceptable. Eventually, the $f–P$ droop loop regulates the phase angle and generates the control signal via an integral controller for the other control blocks. Thus, a restoration in frequency is theoretically conflicting the idea of active power sharing as the active power production is sensitive to the phase angle. This distinguishable phenomenon of frequency restoration can bring a significant inaccuracy in active power sharing.

In order to maintain the stability and frequency of the system, there should be sufficient active power to execute the frequency restoration controller. The load frequency control in a photovoltaic (PV) generation-based inertialess system can be achieved by sharing the active power with neighboring CMGs. The development of a control approach for smooth reconnection of neighboring CMGs without sacrificing the precision of power sharing and system frequency would be very beneficial.

This article proposes a methodology for seamless reconnection between neighboring CMGs using self-synchronization control based on a double-layered droop-controlled (DLDC) approach. The suggested method restores the system's frequency to its nominal value while also precisely sharing the available power. In this perspective, the main contribution of this research is abridged as follows.

1) The DLDC is designed by adding a self-synchronized feature to enable parallel shifting of the $f–P$ slope to restore the operating frequency to its nominal value. The difference in frequency ($\Delta\omega$) will then shift the voltage axis appropriately through the change in V_d and V_q reference of the terminal voltage for appropriate power sharing.
2) A seamless reconnection of neighboring isolated CMGs is proposed in order to support each other, in the case of any power contingency. Both the CMGs are able to support the local loads as well as the neighboring CMG loads. The seamless reconnection feature of the isolated CMGs is the distinctive feature of this article.
3) A unique processor in the loop (PIL) hardware model has been developed in order to verify the accuracy of the proposed controller. OPAL-RT and PLECS hardware simulator has been used to design the power circuit, and the controller is designed on the TI-based F28069M microprocessor.

The rest of this article is organized as follows. Section II describes the detailed control feature of the developed system. Sections III and IV illustrate the mathematical model and stability analysis of the proposed controller, respectively. Section V discusses the complete working principle of the proposed system, and Sections VI and VII show the efficacy of the proposed controller with the help of simulated and real-time experimental results.

II. Design of the Proposed Controller

In this section, the complete design of the proposed controller has been presented, which will be used in the subsequent system development. Fig. 1 shows a generalized schematic representation for two adjacent, isolated CMGs. Both CMGs are presumed to be PV-based MGs, with BESS serving as a backup power source in each of the two CMGs. Each of the CMGs has its own set of local loads to manage. In the subsequent section, the properties of the primary voltage and current control have been analyzed, and furthermore, the distributed secondary control objectives have been proposed to achieve the purposes.

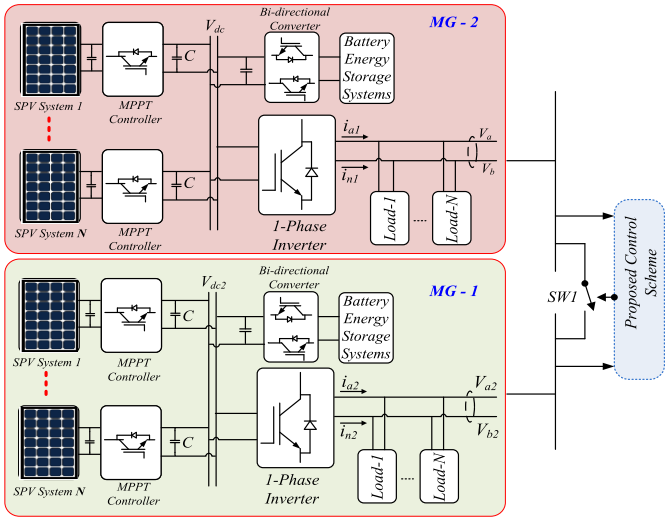

Fig. 1. Structures of CMGs under study.

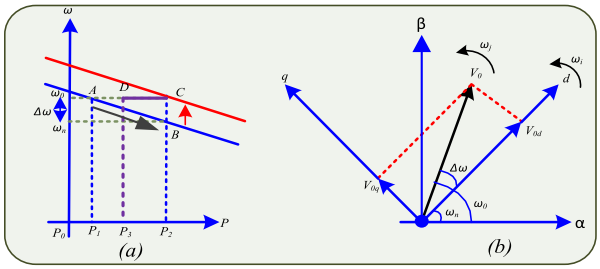

Fig. 2. Proposed improved DLDC.

A. Control Objectives

The state of the art of the proposed research area indicates that the frequency of any isolated microgrid primary controller with the droop function will deviate from its nominal value as long as the total nominal power output is different from the consumption of real power. Furthermore, to connect the isolated neighboring CMGs, a proper connection and disconnection topology has to be designed. Thus, a secondary controller is required to restore the frequency and achieve a seamless connection/disconnection. In order to summarize this, the control objectives of this research article are given as follows-

1) Restore the frequency to its nominal value, i.e.,

$$\lim_{t\to\infty} \omega_i(t) = \omega_0 \quad \forall i \in N \tag{1}$$

Also, to ensure the real power-sharing accuracy, i.e.,

$$\frac{P_{\mathrm{MG}i}}{P_{\mathrm{MG}k}} = \frac{k_{\omega i}}{k_{\omega k}} \quad \forall i,\ k \in N \tag{2}$$

where $k_{\omega i}$ and $k_{\omega k}$ are the active power droop gain of the i^{th} and k^{th} CMG inverter, respectively. This value can be chosen according to the distributed generator (DG) rating [29]. In primary control, the frequency droop gain is usually chosen as the inverse proportion of power rating.

2) Design a seamless connection/disconnection between the isolated CMGs.

B. Distributed Secondary Controller Design

A distributed secondary controller has been proposed in this research work. The proposed secondary controller restores the system frequency to its nominal value and helps for the seamless reconnection of the CMGs and the available active power sharing. The secondary controller generates the frequency and voltage control inputs for the primary controller.

1) Frequency Restoration and Power Sharing: The main focus of this part of the secondary control is to restore the frequency to its nominal value and to improve the active power-sharing accuracy. The conventional frequency droop control ($f-P$), as shown in (3), is a very well-known and established technique for power sharing. A disadvantage of this technique is the nominal value of frequency and voltage changes if output active and reactive power is a deviation from its nominal value (P_0). If the ratio of active/reactive power varies, the voltage and frequency fluctuate, which can cause improper power sharing between CMGs. This is the most important tradeoff between transient responsiveness and stability: deciding how much gain to use [29].

In order to solve this problem, improved droop control is proposed, as shown in Fig. 2(a). The deviation of active power from its nominal value can be compensated on its own by shifting the $f-P$ droop line to restore the system frequency. By shifting this, the system frequency can be controlled to its rated value individually in each CMG. To eliminate the frequency deviation, a correction factor is added to the frequency droop equation in terms of a time-varying filter of the frequency error ($\Delta\omega$).

Fig. 2(a) shows the droop control frequency restoration example of the participating inverter of the CMG. Initially, when the inverter operates in the standalone mode, point A, with frequency ω_0, provides the active power P_1. Due to the change of any load demand, the frequency drifts to ω_n (point B). At that moment, the power supplied by the inverter is P_2. After activating the frequency restoration control, the frequency droop gain is adjusted (to the C point) such that the system frequency returns to its nominal value, preserving the inverter's power output. The same topology is adopted for both the synchronizing isolated inverter of the CMGs. This frequency restoration feature eventually reduces the phase angle error between the participating inverters. This acts as a natural "presynchronization" step, without requiring any additional control action for that. The droop line may be changed to point D once the seamless coupling controller is engaged to achieve precise power sharing as per common demand.

In conventional droop control for the i^{th} inverter

For $f-P$ Droop Control:

$$\omega_n - \omega_0 = -k\omega(P_n - P_o) \tag{3}$$

$$\omega_n - \omega_0 = -k_\omega \Delta P \Rightarrow \Delta\omega = -k_\omega \Delta P \tag{4}$$

where k_ω is the $f-P$ droop coefficient, and when the active power is P_n, the frequency is ω_n.

Furthermore, the instantaneous power of the i^{th} CMG inverter (P_i) can be calculated as

$$P_i = \frac{\omega_c}{S+\omega_c}\left(V_{\text{oid}} I_{\text{oid}} + V_{\text{oiq}} I_{\text{oiq}}\right) \tag{5}$$

or can be written as

$$P_i = \frac{\omega_c}{s+\omega_c} P_i(s) \tag{6}$$

where s is the Laplace operator, $P_i(s)$ is the instantaneous value of the CMGs power, and ω_c is the cutoff frequency for the power calculation filter. V_{oid}, V_{oiq}, I_{oid}, and I_{oiq} are the d- and q-axis components of the i^{th} inverter output voltage and current, respectively.

In order to restore the frequency (ω_{01}), a corrective term ($\Delta\omega$) has to be added with the differed value. To represent this mathematically

$$\omega_{01} = \omega_n + \Delta\omega \tag{7}$$

where

$$\Delta\omega = -k_\omega \Delta P_i = -k_\omega V_{\text{oid}} \Delta I_{\text{oid}} \tag{8}$$

For the control requirement, in order to maintain the unity power factor, as the I_{oiq} reference is zero, the change in active power (ΔP_i) could be represented as the change in the d-axis component of the current (ΔI_{oid}), if the V_{oid} is kept constant, which is the case in the present scenario.

Now, assuming $K_p = -k_\omega V_{\text{oid}}$ so that

$$\Delta\omega = K_p(t) \Delta I_{\text{oid}} \tag{9}$$

Finally,

$$\omega_{01} = \omega_n + K_p \Delta I_{\text{oid}} \tag{10}$$

Furthermore, in the Laplace domain, (4) and (7) can be written as

$$\omega_{01}(s) = \omega_0(s) - k_\omega \frac{\omega_c}{s+\omega_c} \Delta P_i(s) + \Delta\omega \tag{11}$$

Equation (11) can be written as

$$\omega_{01}(s) = \omega_0(s) - k_\omega \frac{\omega_c}{s+\omega_c} P_i(s) + \frac{K_g \omega_s}{s+\omega_s}(\omega_0(s) - \omega_{01}(s)) \tag{12}$$

where ω_s is the additional filter cutoff frequency and K_g is its time-varying gain. It is interesting to further expand the following equation:

$$\omega_{01}(s) = \omega_0(s) - k_x(s) \frac{\omega_c}{s+\omega_c} P_i(s) \tag{13}$$

where $k_x(s) = k_\omega(s+\omega_s)/(s+(1+K_g)\omega_s)$

Hence, the proposed droop control is a modified version of the traditional droop control. The performance of the proposed controller is dependent on the time-varying gain K_p, which is further dependent on the d-axis component of the terminal voltage. The phase angle adjustment through the self-restoration features of the participating inverters is described graphically in Fig. 2(b). The idea is to restore the frequency to its nominal value in order to correct the phase discrepancy. The frequency restoration process, as described in Fig. 2(a) and in the above section, helps both the isolated inverters to operate closely to the nominal frequency. After achieving the synchronization, $\Delta\omega$ should be equal to zero, and at that moment, the q-axis component (V_{oq}) also becomes zero. In this way, phase synchronization is accomplished by restoring the system's frequency to its nominal value. The simplified structure of the proposed controller has been presented in Fig. 3.

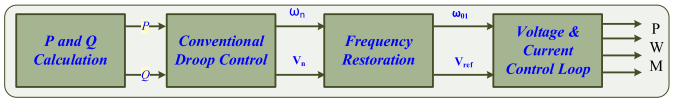

Fig. 3. Block diagram of the proposed control topology.

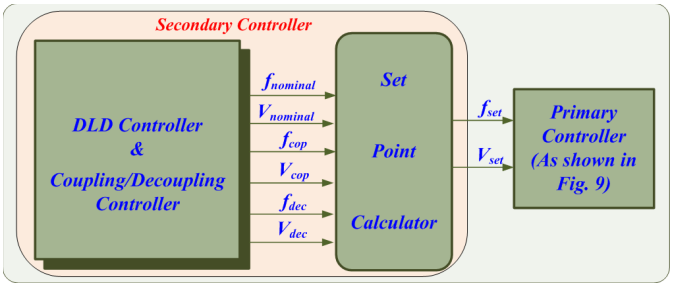

Fig. 4. Proposed frequency–voltage controller for seamless connection.

C. Control Topology for Seamless (De)Coupling of Neighboring CMGs

The previous section discusses how the restoration of system frequency eventually helps to self-synchronize the CMG inverters. CMGs will be used in one of the two ways to conduct this study: either independently (meeting just its own load requirement) or linked with other CMGs. In the case of operating in standalone mode, the proposed control layout (as shown in Fig. 3) defines the operating frequency and voltage as per the nominal value of the set points. However, in interconnection mode, a secondary control architecture is required for power management and protection. The proposed secondary control layout for the voltage and frequency set point calculation is presented in Fig. 4. For a smooth transition between standalone mode and interconnected mode, a connection and disconnection strategy is presented as depicted in Fig. 5. This secondary control scheme produces the necessary frequency and voltage deviation for a smooth transition between standalone mode and interconnected mode. These voltage and frequency deviations for coupling and decoupling (V_{cop} and f_{cop} for coupling and V_{dec} and f_{dec} for decoupling) contribute to defining the new set points of the primary controller's voltage and frequency.

As the CMGs are also capable of working in standalone modes, the voltage and frequency set points should be defined by the local controllers. Fig. 4 shows the final set point calculation for each CMG. When the enable signals are high in the coupling and decoupling controller, the frequency and voltage deviation are produced and are added up with the nominal value of voltage and frequency to define the final set point value of the primary controller.

1) Coupling Controller: The foremost function of the coupling controller is to ensure a smooth transition between

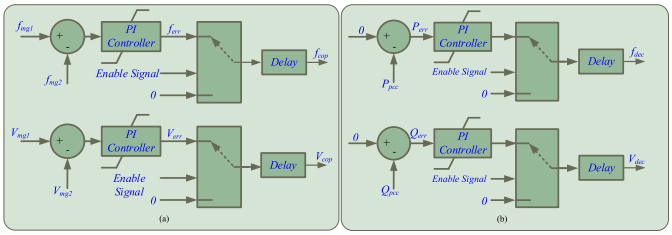

Fig. 5. Layout of (a) coupling and (b) decoupling controller.

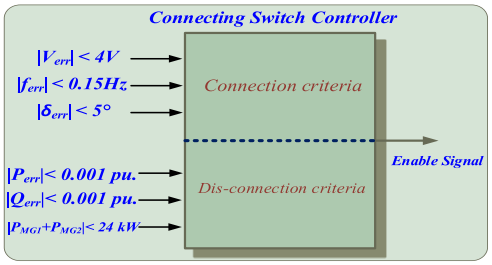

Fig. 6. Connection and disconnection criteria.

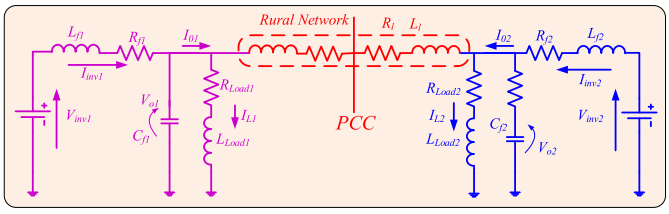

Fig. 7. Equivalent circuit and power flow of coupled CMG.

standalone mode and interconnected mode without affecting the performance of each individual CMG. In the standalone mode, the voltage and the frequency set points are governed by the proposed self-synchronized controller, and for the interconnection, the parameters of both the CMGs must be adapted to match all the values before the actual closure of the contactor switch. Fig. 5 shows a synchronization concept that is used to eliminate any aberrant transient behavior and transition instability. The difference in voltage magnitude, frequency, and phase of the voltage of two microgrids is reduced to the very low limit for the seamless transition of modes. The magnitude of the error value is reduced by designing a suitable proportional–integral (PI) controller.

As shown in Fig. 5(a), the coupling controller consists of a voltage error and frequency error controller. Coupling of two systems with a large voltage magnitude difference can cause a voltage drop in a coupled system. In order to match the voltage of two CMG, the voltage difference between the two microgrids is fed to the PI controller. The PI controller attempts to minimize this error by bringing the voltages of the two systems as near as feasible. The selected signal is passed through a first-order filter to generate the final voltage deviation, V_{cop}. Similarly, the frequency error signal of both the CMG is passed through a PI controller to minimize the error, and finally, f_{cop} is generated to create the final frequency deviation. Another criterion for coupling is to reduce the phase angle difference. The integral of frequency difference over time produces the relative phase angle. Thus, practically minimizing the frequency deviation actually minimizes the phase error as well.

2) Decoupling Controller: The decoupling controller guarantees a smooth and flawless transition from interconnected mode to standalone mode and also ensures that the accompanying disturbances in the standalone system are minimal. The standalone CMG systems also have some limitations, e.g., they cannot be overloaded for an indefinitely long time, and if the local load demand increases beyond the capacity of the coupled system, then it is advised to bring back the coupled CMG to the standalone mode for individual load shedding purposes.

Fig. 5(b) shows the layout of the decoupling controller. The active power and reactive power at the coupling point are measured and compared with zero, and the error signal is passed through a PI controller to generate the voltage and frequency deviation V_{dec} and f_{dec}.

3) Connection/Disconnection Criteria: Once all the error signals are within acceptable limits for a minimum period of ten cycles (∼0.2 s), the associated enable signal is triggered, and seamless coupling of neighboring microgrids is established. Similarly, the controller is prepared for the system disconnection when P_{err} and Q_{err} fall below 0.001 p.u. and the power of CMG1 and CMG2 exceeds their rated values. Fig. 6 shows the connection and disconnection criteria for the coupling and decoupling controller.

III. Mathematical Model of the Proposed Controller

In this section, the mathematical modeling and the stability analysis of the proposed system have been discussed. Fig. 7 shows the simplified structure of interconnected standalone CMG. The equivalent circuit diagram consists of two voltage sources, *LC* filter, rural network, and loads. The simplified controller structure with voltage and current control loop, droop control, and double-layered frequency restoration control is depicted in Fig. 3. In this section, the mathematical model of each individual component of the control structure is developed. The active power control between the CMGs is generally achieved by changing the phase angle between the CMG inverters. This is usually accomplished by using droop control where the frequency is regulated by using the droop equation as follows:

$$\omega_1 = \omega_0 - k_\omega \Delta P \tag{14}$$

where k_ω is the droop gain, ω_1 is the output frequency of the CMG1, ω_0 is the nominal frequency, and ΔP is the power supplied from CMG1 to CMG2 (or vice versa). The phase angle difference is modified according to the function of power supplies to another CMG. The phase angle difference between the CMGs can be defined as follows:

$$\Delta\delta_i = \int (\omega_i - \omega_j) dt \tag{15}$$

In (15), ω_i and ω_j are the final output frequency of CMG1 and CMG2, respectively.

In the coupled system (they will be adopted to a common frequency) in case of any load change, the output frequency will change and will settle down in a steady-state frequency. The settled steady-state frequency is most likely to differ from

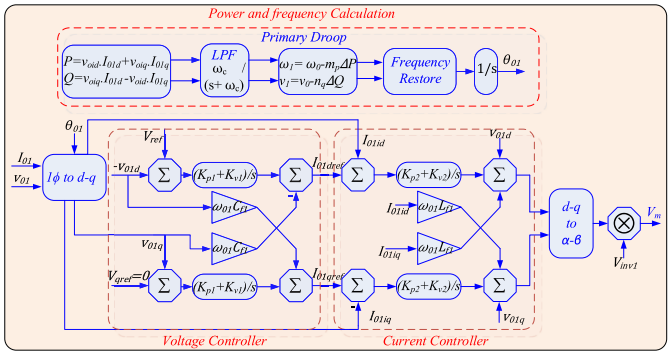

Fig. 8. Proposed CMG inverter controller.

the nominal value ω_0. In order to restore the frequency, a restoration technique (DLDC) has been proposed.

The required amount of frequency component (let us say, $\Delta\omega$) to restore the frequency is determined by the d-axis component of the output voltage (as derived in Section II-B). The frequency of coupled system after restoration will be

$$\omega_{01} = \omega_1 + \Delta\omega \tag{16}$$

Each interfacing inverter of the CMGs has a voltage and current control loop implemented in the d–q coordinates. The internal voltage control loop generates the d-and q-axis current references for the current controller. As both the current and the voltage control loop operate in the d–q coordinates, a PI controller is implemented. The electrical phase angle θ_{01} is generated by integrating the output frequency of the coupled system

$$\theta_{01} = \int (\omega_1 + \Delta\omega)dt = \int \omega_{01}dt \tag{17}$$

Fig. 8 shows a complete architecture of the control topology implemented for each inverter in CMG.

The state equations of the primary voltage and current controllers are already available in different literature [30], [31], [32]. In the following sections, a detailed analysis of all the controllers is presented.

As stated earlier, the proposed controllers are designed in the d–q reference frame, so

$$I_{01} = I_{01\alpha} + jI_{01\beta} \tag{18}$$

$$I_{01}e^{-j\theta 01} = I_{01d} + jI_{01q} \tag{19}$$

$$I_{01} = (I_{01d} + jI_{01q})e^{j\theta 01} \tag{20}$$

The transformation of α–β frame to d–q frame is shown in the previous equation, where θ_{01} is obtained from (17).

The state-space equations of each inverter output current, filtered voltage, and load current are shown as follows.

$$\Delta I_{\text{inv1d}} = \omega_{01}\Delta I_{\text{inv1q}} + \Delta\omega_{01}I_{\text{inv1q}} - \frac{R_{f1}}{L_{f1}}\Delta I_{\text{inv1d}} + \frac{\Delta v_{\text{inv1d}}}{L_{f1}} - \frac{\Delta v_{01d}}{L_{f1}} \tag{21}$$

$$\Delta I_{\text{inv1q}} = -\omega_{01}\Delta I_{\text{inv1d}} - \Delta\omega_{01}I_{\text{inv1d}} - \frac{R_{f1}}{L_{f1}}\Delta I_{\text{inv1q}} + \frac{\Delta v_{\text{inv1q}}}{L_{f1}} - \frac{\Delta v_{01q}}{L_{f1}} \tag{22}$$

$$\Delta\dot{L}_{L1d} = \omega_{01}\Delta I_{L1q} + \Delta\omega_{01}I_{L1q} - \frac{R_{\text{Load1}}}{L_{\text{Load1}}}\Delta I_{L1d} + \frac{\Delta v_{01d}}{L_{\text{Load1}}} \tag{23}$$

$$\Delta\dot{L}_{L1q} = -\omega_{01}\Delta I_{L1d} - \Delta\omega_{01}I_{L1d} - \frac{R_{\text{Load1}}}{L_{\text{Load1}}}\Delta I_{L1q} + \frac{\Delta v_{01q}}{L_{\text{Load1}}} \tag{24}$$

$$\Delta\dot{v}_{01d} = \omega_{01}\Delta v_{01q} + \Delta\omega_{01}v_{01q} + \frac{\Delta I_{\text{inv1d}}}{C_{f1}} - \frac{\Delta I_{01d}}{C_{f1}} \tag{25}$$

$$\Delta\dot{v}_{01q} = -\omega_{01}\Delta v_{01d} - \Delta\omega_{01}v_{01d} + \frac{\Delta I_{\text{inv1q}}}{C_{f1}} - \frac{\Delta I_{01q}}{C_{f1}} \tag{26}$$

The transmission line dynamics are shown in the following state-space equations:

$$\left.\begin{aligned}\Delta\dot{I}_{01d} &= \omega_{01}\Delta I_{01q} + \Delta\omega_{01}I_{01q} - \frac{R_l}{L_l}\Delta I_{01d} \\ &+ \left(\frac{1}{L_l} + \frac{1}{L_{\text{Load}}}\right)\Delta v_{01d} - \frac{v_{02d}}{L_l} + \left(\frac{R_l}{L_l} - \frac{R_{\text{Load}}}{L_{\text{Load}}}\right)\Delta I_{L1d}\end{aligned}\right\} \tag{27}$$

$$\left.\begin{aligned}\Delta\dot{I}_{01q} &= -\omega_{01}\Delta I_{01d} - \Delta\omega_{01}I_{01d} - \frac{R_l}{L_l}\Delta I_{01q} \\ &+ \left(\frac{1}{L_l} + \frac{1}{L_{Load}}\right)\Delta v_{01q} - \frac{v_{02q}}{L_l} + \left(\frac{R_l}{L_l} - \frac{R_{\text{Load}}}{L_{\text{Load}}}\right)\Delta I_{L1q}\end{aligned}\right\} \tag{28}$$

The power calculation and droop equations are presented as follows:

$$P = v_{01d}\cdot I_{01d} + v_{01q}\cdot I_{01q} \tag{29}$$

$$Q = v_{01q}\cdot I_{01d} - v_{01d}\cdot I_{01q} \tag{30}$$

The power equations after filter can be written as the following, where ω_c is the filter cutoff frequency:

$$P_1 = \frac{\omega_c}{S+\omega_c}(v_{01d}\cdot I_{01d} + v_{01q}\cdot I_{01q}) \tag{31}$$

$$Q_1 = \frac{\omega_c}{S+\omega_c}(v_{01q}\cdot I_{01d} - v_{01d}\cdot I_{01q}) \tag{32}$$

$$\omega_l = \omega_0 - k_\omega\Delta P \tag{33}$$

$$v_1 = v_0 - k_v\Delta Q \tag{34}$$

The mathematical derivation for the double-layered droop controller can be retrieved from (7) to (13).

Considering all the above equations, the state matrix of a CMG will be

$$X_1 = [\Delta\delta_{01}\ \ \Delta P_1\ \ \Delta Q_1\ \ \Delta I_{L1\text{dq}}\ \ \Delta I_{\text{inv1dq}}\ \ \Delta V_{01\text{dq}}\ \ \Delta I_{01\text{dq}}]^T \tag{35}$$

Similarly, all the equations for another CMG can be obtained and the state-space matrix can be written as

$$X_2 = [\Delta\delta_{02}\ \ \Delta P_2\ \ \Delta Q_2\ \ \Delta I_{L2\text{dq}}\ \ \Delta I_{\text{inv2dq}}\ \ \Delta V_{02\text{dq}}\ \ \Delta I_{02\text{dq}}]^T \tag{36}$$

Finally, the state-space matrix for coupled CMG can be written as

$$X = \begin{bmatrix} X_1^T\ \ X_2^T \end{bmatrix}^T \tag{37}$$

A fixed communication delay for exchanging information among the DGs and primary and secondary controllers has been considered. The linear distributed control law for voltage

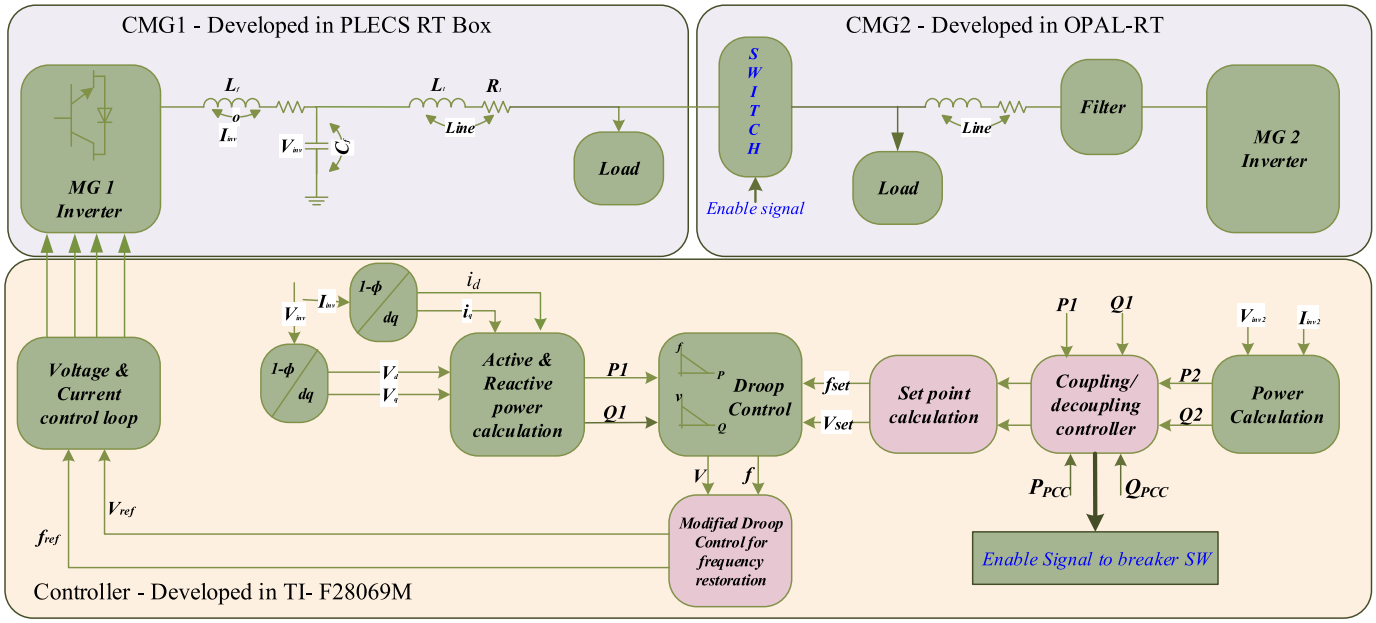

Fig. 9. Development of the proposed system with improved controllers.

and frequency control with delay has been shown in the following:

$$\left.\begin{aligned}\Delta\omega_{0i} &= -c_1 * L * \omega_{0i}(t-t_d)\\ &+ c_1 * G * \left(I * \omega_{ref} - \omega_{0i}\right) - c_2 * L * k_\omega P_i(t-t_d)\end{aligned}\right\} \quad (38)$$

$$\left.\begin{aligned}\Delta V_{0i} &= -c_3 * L * V_{0i}(t-t_d)\\ &+ c_3 * G * \left(I * V_{ref} - V_{0i}\right) - c_4 * L * k_v Q_i(t-t_d)\end{aligned}\right\} \quad (39)$$

where L and G are the Laplacian matrix and gain matrix of the system, respectively; c_1, c_2, c_3, and c_4 are the control gains; and t_d is the communication delay. The calculated delayed active power can be represented as

$$P_i(t-t_d) = V_{0id}(t-t_d)i_{0id}(t-t_d) + V_{0iq}(t-t_d)i_{0iq}(t-t_d) \quad (40)$$

$$Q_i(t-t_d) = -V_{0id}(t-t_d)i_{0iq}(t-t_d) + V_{0iq}(t-t_d)i_{0id}(t-t_d) \quad (41)$$

The state equations of the delayed secondary controllers are given as follows:

$$[\Delta\dot{\omega}_{\mathrm{MG}i}] = A_{D\Omega}[\Delta X_i(t)] + B_{D\Omega}[\Delta X_i(t-t_d)] + C_{D\Omega}\Delta\omega_{\mathrm{ref}} \quad (42)$$

$$\left[\Delta\dot{V}_{\mathrm{MG}i}\right] = A_{D\lambda}[\Delta X_i(t)] + B_{D\lambda}[\Delta X_i(t-t_d)] + C_{D\lambda}\Delta V_{\mathrm{ref}} \quad (43)$$

where $A_{D\Omega}$, $B_{D\Omega}$, $C_{D\Omega}$, $A_{D\lambda}$, $B_{D\lambda}$, and $C_{D\lambda}$ are the system coefficient matrix.

IV. Stability Analysis Through Eigenvalues

The eigenvalues shown in Table I are mainly sensitive to droop controller parameters, load demand, transmission line parameters, and gains of state feedback controllers. The dominant eigenvalues with the variation of different parameters are analyzed in detail in the following section.

TABLE I
System Eigenvalues

Real	Img.	Damping Ratio
-870.913	±180.29	100
-503.287	±1.09*10e4	11.46
-293.616	±1.13*10e4	26.19
-296.768	±39.46	86.31
-101.544	±24.83	51.46
-102.129	±6.894	57.16
-49.725	0	98.9
-880.21	±201.59	99.98
-506.964	±1.171*10e4	25.48
-291.569	±1.276*10e4	27.4
-295.619	±37.49	87.5
-106.583	±33.73	58.6
-104.237	±7.547	60.4
-50.59	0	99.5

The coupled system is linearized around an operating point and all the eigenvalues are shown in Table I. The corresponding damping ratio is also calculated. All the eigenvalues can be divided into two groups—well-damped eigenvalues and potentially problematic eigenvalues. The eigenvalues with damping ratios less than 30% are considered as problematic eigenvalues, as these are not damped quickly. The oscillations created due to these values eventually affect the system performance. The consequences due to these oscillations can result in loss of efficiency, control system instability, and mainly wear and tear on equipment. Oscillations in output voltage and current can create harmonics and affect the power quality. The proposed secondary controller with a fixed communication delay has less number of problematic eigenvalues and maintains the system stability. In order to further improve the system stability, a predictive/robust controller design is required, as has been duly acknowledged in the scope of extension of the work in future.

TABLE II
CMG PARAMETERS

System Parameters	
Dc Link Capacitor	2000 μF
Filter Inductor (L1)	8.5 mH
Filter Capacitor	30 μF
Power Rating for CMG1 Inverter	10 kW
Power Rating for CMG2 Inverter	10 kW
BESS Capacity in CMG1	5 kWh
BESS Capacity in CMG 2	5 kWh
Frequency drooping gain	0.05 rad/s/W
Voltage drooping gain	0.01 V/Var

V. WORKING PRINCIPLE

The integration technique of the proposed DLDC with the coupling and decoupling controller is presented in Fig. 9. In order to make it compact, the detailed control topology of CMG1 participating inverter control is only shown in Fig. 9, whereas the participating inverter of the CMG2 adopts the same control topology. The set points of voltage and frequency from the secondary controller are given to the primary voltage and current controller of the interfacing inverter. In the case of standalone mode, both the CMGs operate on its own and deliver the power to the local load, but in the interconnected mode, both the microgrids deliver the total load connected to it, and the power is shared according to the droop controller.

VI. SIMULATION STUDIES

The proposed control strategies for frequency restoration and seamless (de)coupling between the neighboring CMGs, as described in the previous sections, are assessed and verified in this section. To prove the efficacy of the proposed controllers, the scaled-down prototype of the two PV-based single-phase CMGs is developed, and five different case studies are considered. In each CMG, the PV systems are connected to the interfacing inverter through a dc/dc boost converter. Furthermore, the CMG inverter is interfaced to the local load through an *LC* filter, as shown in Fig. 9. Different case studies, such as seamless coupling, decoupling, and reconnection again after the decoupling, have been showcased to demonstrate the proposed controller's efficacy. In real time, any of the modes will be activated and act as per the requirement. The transition from one to another will be determined according to the proposed control topology. All the system parameters in normal operating condition in standalone mode are shown in Table II. MATLAB SimPowerSystem is used to develop the detailed model of the CMGs.

A. Normal Operation With Frequency Restoration

In this case study, two distinct scenarios were investigated to demonstrate the effectiveness of the proposed modified double-layered droop controller. In the first one, both the microgrids are connected with 4-kW load individually. At the simulation time instant 1 s, both the loads are increased to 5 kW, and the effectiveness of the proposed controller is analyzed. The voltage and current profile of the CMG1 is shown in Fig. 10. It can be observed that both voltage and current are in phase and voltage amplitude remains stable after load change. In the second situation, both the CMGs are connected to 7-kW loads, and at the simulation time instant 1 s, both the loads are increased to 11 kW. Fig. 11 shows the power and frequency profile of the CMG2. A comparison is shown in the frequency profile with the proposed DLDC and conventional droop control. According to the simulation results, the frequency profile of the suggested droop control is considerably smoother and more stable than that of traditional droop control. The frequency profile with conventional droop control is oscillating in nature during any transient; however, both the frequencies are within the acceptable limit.

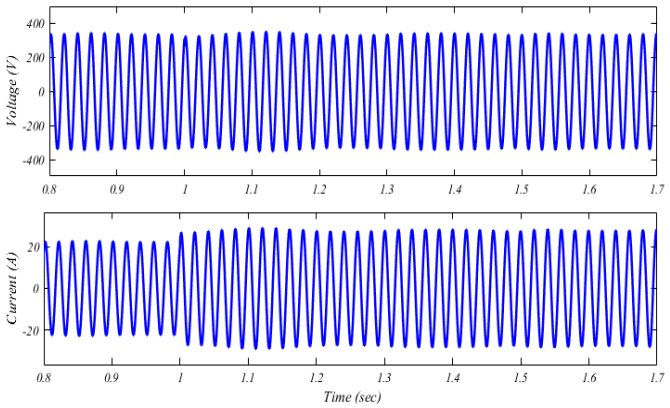

Fig. 10. Voltage and current profile of CMG1.

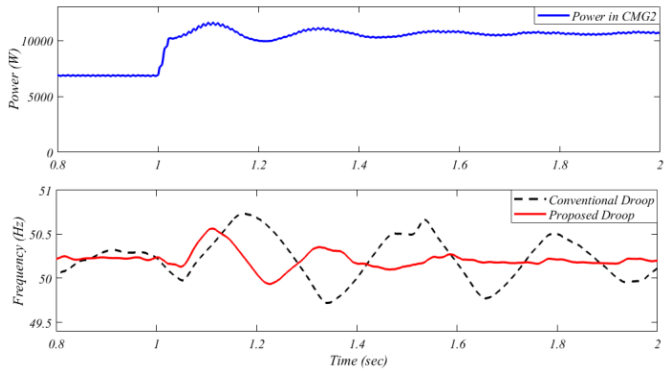

Fig. 11. CMG2 load demand and frequency profile.

B. Seamless Interconnection of Microgrids

As discussed in Section III, a control topology is developed to demonstrate a smooth, seamless transition from standalone mode to interconnected mode. When the enable signal of the coupling controller is triggered, the controller generates the required frequency and voltage deviation for the seamless transition, which contributes to defining the final voltage and frequency set point values of the CMG inverters. After checking the required connection criteria, as shown in Fig. 6, the breaker connecting to the network and both the CMGs come to coupled condition.

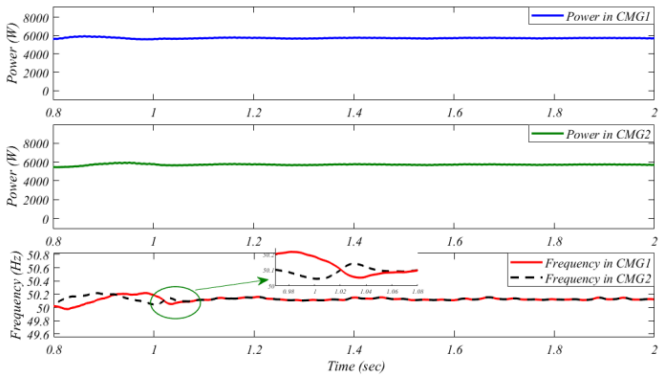

Fig. 12. Illustration of the seamless interconnection of CMGs.

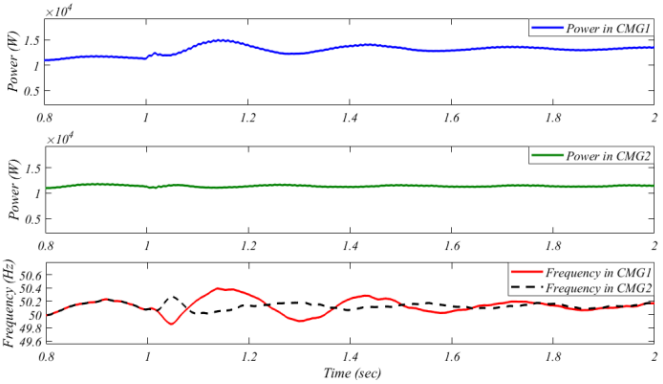

Fig. 14. Illustration of seamless decoupling.

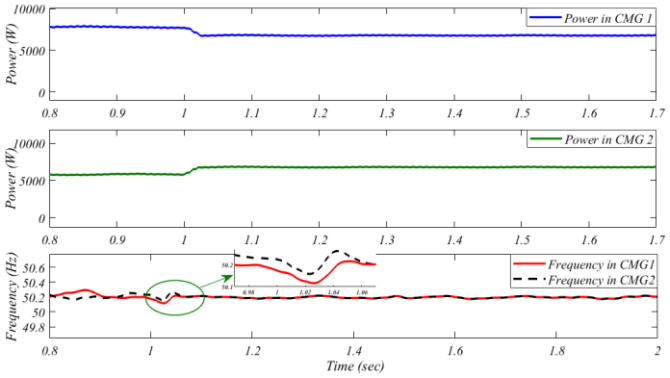

Fig. 13. Power sharing performance in an interconnected mode.

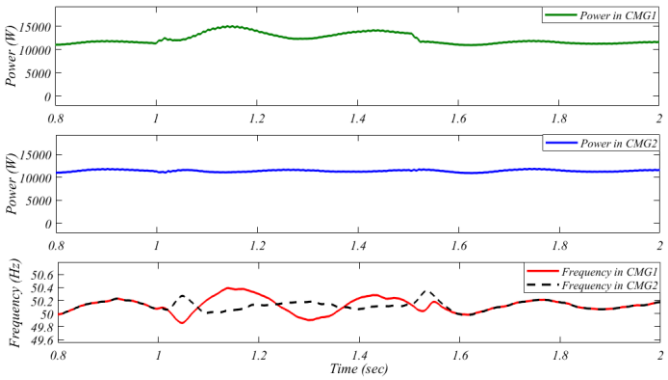

Fig. 15. Reconnection of CMGs after decoupling.

To check the efficiency of the proposed controller, both the CMGs are connected to the 6-kW load, and at the simulation time 1 s, the coupling controller enable signal is triggered. As shown in Fig. 12, both the CMGs are delivering 6-kW load demand, and they have their own different frequency profile, but after getting coupled at 1 s, both have the same frequency profile. As we can see from the frequency profile, the coupled system takes only 0.05 s to stabilize without affecting the local load demand requirement of the individual CMG.

C. Power-Sharing Performance in an Interconnected Mode

This case study illustrates the power-sharing performance of the proposed controller after interconnecting the CMGs. In order to demonstrate that, the CMG1 is connected to the 8-kW load, and CMG2 is connected to the 6-kW load. They are supplying their own load demand up to 1 s of the simulation time. At this time, the enable signal of the coupling controller is triggered. After coupling, both the CMGs share the total load demand, and as a result, both the CMGs contribute 7 kW each (as the total load demand is 14 kW) to the total load demand. The power-sharing performance of the CMGs is shown in Fig. 13. It is also worth noting that the seamless coupling is accomplished without compromising the proposed controller's power-sharing capabilities.

D. Seamless Decoupling of the CMGs

The main objective of the decoupling controller is a seamless transfer of coupled CMGs to a standalone CMG without affecting the system stability. In this case study, initially, both the CMGs have a 12-kW load demand. In this condition, another 2-kW load demand is increased in CMG1 then; according to the control architecture provided in Fig. 6, the decoupling controller triggered automatically. As soon as all of the conditions for disconnecting have been met, the breaker is activated, and both CMGs are isolated. As shown in Fig. 14, both the CMGs are supplying 24-kW load demand initially, and at 1-s simulation time when the CMG1 load demand is increased by 2 kW, the disconnection controller operates; without affecting the system stability, a seamless disconnection occurs. The system frequency was maintained after the disconnection and the CMGs are supplying the local load demand individually.

E. Reconnection After Decoupling

In this case study, a reconnection is attempted immediately after a disconnection occurs, to check the efficacy of all the proposed controllers. Like the previous case study initially, the load demand of both the CMGs is 12 kW, and at the simulation time 1 s, 2-kW load demand in CMG1 is increased. In this situation, the decoupling controller operates and decouples the CMGs. Immediately after that, at simulation time 1.5 s, the excess 2-kW load demand is reduced, and again, the coupling controller enable signal is triggered and the seamless coupling is achieved in 0.03 s. As shown in Fig. 15, throughout the simulation, the frequency remains in the allowable range, which enables a seamless reconnection again.

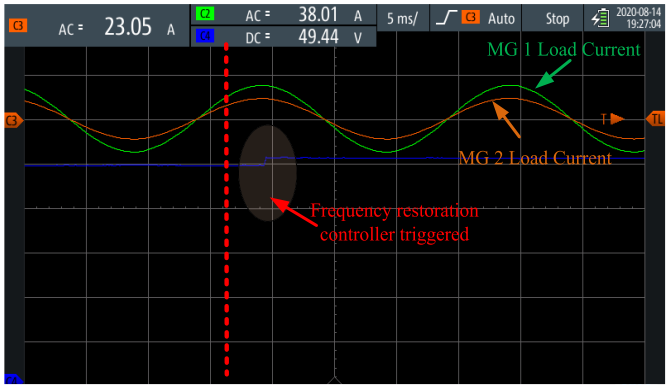

Fig. 16. Illustration of frequency restoration controller.

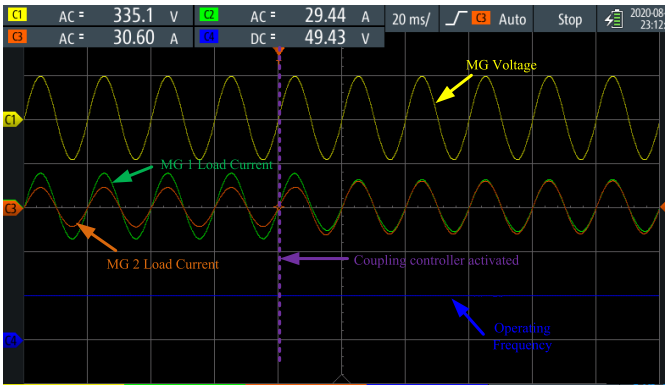

Fig. 17. Illustration of seamless coupling of CMGs.

VII. Experimental Validation

To demonstrate the efficacy of the proposed controllers, a unique laboratory prototype is developed. In the developed PIL hardware design, PLECS RT box and OPAL-RT along with the Texas Instrument-based F28069M microcontroller is utilized. In PIL applications, the power stage of CMG1 is emulated in the PLECS RT box, and the power stage of breaker with CMG2 is implemented in the OPAL-RT simulator. The digital signal processor F28069M connected to the PLECS RT box with breakout board is used to design the proposed controllers of the system. Due to page constraints, only critical case studies have been shown in this section.

A. Normal Operation With Frequency Restoration

The processor in loop experimental result, as shown in Fig. 16, provides a normal operating condition of isolated CMGs, where both the CMGs are supplying their individual loads. In this scenario, CMG1 and CMG2 are supplying 38 A (∼12.5 kW) and 23 A (∼8 kW) of load current individually, while the frequency is maintained within the acceptable limit. Now, in order to restore the frequency, the frequency restoration controller is triggered. As captured in Fig. 16, shown in the zoomed frequency plot, the frequency is restored to its nominal value. It can be also observed that the frequency is restored, while the converter continues to supply the same load demand. Thus, the experimental results provide a satisfactory test of frequency restoration controller.

B. Seamless Coupling of CMGs and Power-Sharing Performance

In this case study, the desired load demand is first supplied by both CMGs individually before the coupling controller is activated. As shown in Fig. 17, both the CMGs are coupled seamlessly, without creating any sudden transient in the voltage/current profile. As can be seen, the frequency is likewise kept within tolerable bounds. These results also demonstrate how well droop controller performs in a power-sharing scenario. Once the CMGs are coupled, it is clear that the entire load current is split evenly between them. This case study provides satisfactory testing of the proposed seamless coupling and droop controller.

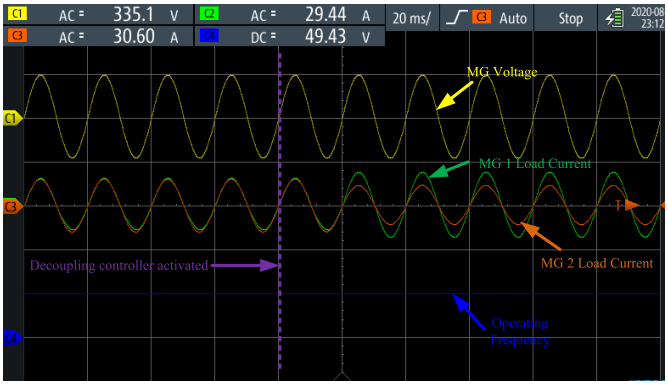

Fig. 18. Illustration of seamless decoupling of CMGs.

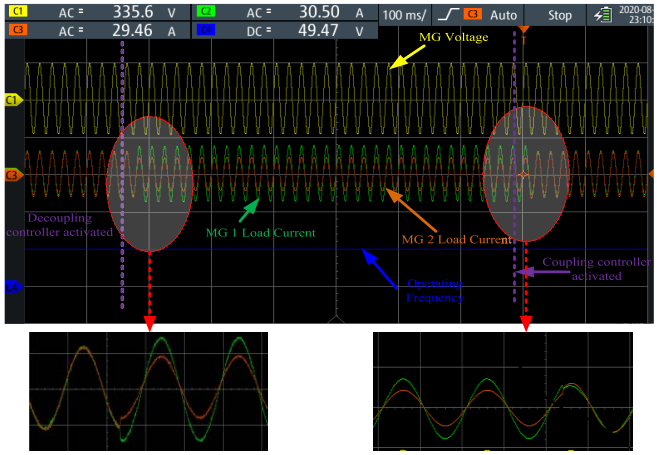

Fig. 19. Illustration of seamless reconnection of CMGs.

C. Seamless Decoupling of CMGs

The decoupling controller's effectiveness was tested in this case study using a similar strategy. When both CMGs are first linked, the entire load demand is split evenly between them. When the decoupling controller is activated, the CMGs decouple and provide each CMG load requirement separately. Fig. 18 shows that the decoupling is smooth and that the system stability is maintained without causing any abrupt transients in the voltage/current profile. It can also be observed that seamless decoupling is achieved in one switching cycle.

D. Reconnection After Decoupling

After decoupling, reconnection is sought and successfully accomplished in this case study. The system experiences a seamless transition from standalone to linked mode. The zoomed plot, as shown in Fig. 19, proves the efficacy of the proposed controller. Besides, it is worth underlining that both the coupling and decoupling controller response in one switching cycle, i.e., in 0.02 s which is according to the IEEE standard 1547.4-2011 and IEEE 1547.2-2008 for reconnection.

VIII. Conclusion and Scope of Future Work

This article proposes an improvement in droop control to restore the system frequency to its nominal value, allowing the CMG to self-synchronize with the adjacent one. The extra layer in the proposed droop control uses the d-axis component of the terminal voltage to maintain the system frequency and voltage for seamless reconnection. The results of a MATLAB-based simulation and a PIL-based real-time implementation for a number of potential distinct case studies demonstrate successful implementation of the seamless reconnection of CMGs without compromising the power-sharing accuracy. The major contributions of this article are given as follows.

1) The successful implementation of double-layered self-synchronized droop control, which helps to keep the system frequency close to the nominal value.
2) A mathematical model of the proposed controller considering the communication delay in the distributed secondary controller is presented and the system stability is also analyzed.
3) Different transient conditions, such as load change, coupling to other CMG, and decoupling are considered, and the efficiency of the proposed controller is successfully tested.
4) A seamless coupling and decoupling controller according to the IEEE standard 1547.4-2011 and IEEE 1547.2-2008 is also effectively implemented in this article.
5) The power-sharing accuracy of the proposed droop control is not compromised during any transient situation.

However, in order to restore the frequency, both the present and past frequency control inputs should be equal. Thus, the proposed controller indeed requires the previous values as a reference to execute the controller properly. A robust estimation-based predictive controller can solve this issue and improve the steady-state performance. The design of the robust predictive droop controller is considered in the scope of the future work of this current research work. However, the performance of the proposed controller is also IEEE standard 2030.7 and 2030.8 compliant.

References

[1] E. Dehghanpour, H. K. Karegar, and R. Kheirollahi, "Under frequency load shedding in inverter based microgrids by using droop characteristic," *IEEE Trans. Power Del.*, vol. 36, no. 2, pp. 1097–1106, Apr. 2021.

[2] Z. Li, Y. Xu, X. Feng, and Q. Wu, "Optimal stochastic deployment of heterogeneous energy storage in a residential multienergy microgrid with demand-side management," *IEEE Trans. Ind. Informat.*, vol. 17, no. 2, pp. 991–1004, Feb. 2021.

[3] R. Zamora and A. K. Srivastava, "Controls for microgrids with storage: Review, challenges, and research needs," *Renew. Sustain. Energy Rev.*, vol. 14, no. 7, pp. 2009–2018, Sep. 2010.

[4] R. H. Lasseter, "Smart distribution: Coupled microgrids," *Proc. IEEE*, vol. 99, no. 6, pp. 1074–1082, Jun. 2011.

[5] F. Shahnia, S. Bourbour, and A. Ghosh, "Coupling neighboring microgrids for overload management based on dynamic multicriteria decision-making," *IEEE Trans. Smart Grid*, vol. 8, no. 2, pp. 969–983, Mar. 2017.

[6] E. Pashajavid, A. Ghosh, and F. Zare, "A multimode supervisory control scheme for coupling remote droop-regulated microgrids," *IEEE Trans. Smart Grid*, vol. 9, no. 5, pp. 5381–5392, Sep. 2018.

[7] G. Di Lorenzo, S. Rotondo, R. Araneo, G. Petrone, and L. Martirano, "Innovative power-sharing model for buildings and energy communities," *Renew. Energy*, vol. 172, pp. 1087–1102, Jul. 2021.

[8] *Renewable Energy—Recast to 2030 (RED II)*. EU Science Hub. Accessed: Oct. 17, 2021. [Online]. Available: https://ec.europa.eu/jrc/en/jec/renewable-energy-recast-2030-red-ii

[9] F. Tang, J. M. Guerrero, J. C. Vasquez, D. Wu, and L. Meng, "Distributed active synchronization strategy for microgrid seamless reconnection to the grid under unbalance and harmonic distortion," *IEEE Trans. Smart Grid*, vol. 6, no. 6, pp. 2757–2769, Nov. 2015.

[10] S. D'silva, M. B. Shadmand, and H. Abu-Rub, "Microgrid control strategies for seamless transition between grid-connected and islanded modes," in *Proc. IEEE Texas Power Energy Conf. (TPEC)*, Feb. 2020, pp. 1–6.

[11] K.-H. Tan and T.-Y. Tseng, "Seamless switching and grid reconnection of microgrid using Petri recurrent wavelet fuzzy neural network," *IEEE Trans. Power Electron.*, vol. 36, no. 10, pp. 11847–11861, Oct. 2021.

[12] R. Rosso, S. Engelken, and M. Liserre, "Robust stability analysis of synchronverters operating in parallel," *IEEE Trans. Power Electron.*, vol. 34, no. 1, pp. 11309–11319, Nov. 2019.

[13] Z. Shuai, W. Huang, Z. J. Shen, A. Luo, and Z. Tian, "Active power oscillation and suppression techniques between two parallel synchronverters during load fluctuations," *IEEE Trans. Power Electron.*, vol. 35, no. 4, pp. 4127–4142, Apr. 2020.

[14] C. Jin, M. Gao, X. Lv, and M. Chen, "A seamless transfer strategy of islanded and grid-connected mode switching for microgrid based on droop control," in *Proc. IEEE Energy Convers. Congr. Exposit. (ECCE)*, Sep. 2012, pp. 969–973.

[15] K. De Brabandere, B. Bolsens, J. Van den Keybus, A. Woyte, J. Driesen, and R. Belmans, "A voltage and frequency droop control method for parallel inverters," *IEEE Trans. Power Electron.*, vol. 22, no. 4, pp. 1107–1115, Jul. 2007.

[16] J. He, Y. W. Li, J. M. Guerrero, F. Blaabjerg, and J. C. Vasquez, "An islanding microgrid power sharing approach using enhanced virtual impedance control scheme," *IEEE Trans. Power Electron.*, vol. 28, no. 11, pp. 5272–5282, Nov. 2013.

[17] X. Meng, J. Liu, and Z. Liu, "A generalized droop control for grid-supporting inverter based on comparison between traditional droop control and virtual synchronous generator control," *IEEE Trans. Power Electron.*, vol. 34, no. 6, pp. 5416–5438, Sep. 2019.

[18] Y. Han, H. Li, P. Shen, E. A. A. Coelho, and J. M. Guerrero, "Review of active and reactive power sharing strategies in hierarchical controlled microgrids," *IEEE Trans. Power Electron.*, vol. 32, no. 3, pp. 2427–2451, Mar. 2017.

[19] U. B. Tayab, M. A. Roslan, L. J. Hwai, and M. Kashif, "A review of droop control techniques for microgrid," *Renew. Sustain. Energy Rev.*, vol. 76, pp. 717–727, Sep. 2017.

[20] K. Ş. Parlak, M. Özdemir, and M. T. Aydemir, "Active and reactive power sharing and frequency restoration in a distributed power system consisting of two UPS units," *Int. J. Electr. Power Energy Syst.*, vol. 31, no. 5, pp. 220–226, Jun. 2009.

[21] J. Rey, C. Rosero, M. Velasco, P. Marti, J. Miret, and M. Castilla, "Local frequency restoration for droop-controlled parallel inverters in islanded MGs," *IEEE Trans. Energy Convers.*, vol. 34, no. 3, pp. 1232–1241, Sep. 2019.

[22] F. Guo, C. Wen, J. Mao, and Y. D. Song, "Distributed secondary voltage and frequency restoration control of droop-controlled inverter-based microgrids," *IEEE Trans. Ind. Electron.*, vol. 62, no. 7, pp. 4355–4364, Jul. 2015.

[23] M. Eskandari, L. Li, M. H. Moradi, P. Siano, and F. Blaabjerg, "Active power sharing and frequency restoration in an autonomous networked microgrid," *IEEE Trans. Power Syst.*, vol. 34, no. 6, pp. 4706–4717, Nov. 2019.
[24] G. Chen and Z. Guo, "Distributed secondary and optimal active power sharing control for islanded microgrids with communication delays," *IEEE Trans. Smart Grid*, vol. 10, no. 2, pp. 2002–2014, Mar. 2019.
[25] S. Prakash, V. Nougain, and S. Mishra, "Adaptive droop-based control for active power sharing in autonomous microgrid for improved transient performance," *IEEE J. Emerg. Sel. Topics Power Electron.*, vol. 9, no. 3, pp. 3010–3018, Jun. 2021.
[26] W. Deng, N. Dai, K.-W. Lao, and J. M. Guerrero, "A virtual-impedance droop control for accurate active power control and reactive power sharing using capacitive-coupling inverters," *IEEE Trans. Ind. Appl.*, vol. 56, no. 6, pp. 6722–6733, Nov. 2020.
[27] L. Zhang, H. Zheng, Q. Hu, B. Su, and L. Lyu, "An adaptive droop control strategy for islanded microgrid based on improved particle swarm optimization," *IEEE Access*, vol. 8, pp. 3579–3593, 2020.
[28] Y. Zhu, F. Zhuo, F. Wang, B. Liu, R. Gou, and Y. Zhao, "A virtual impedance optimization method for reactive power sharing in networked microgrid," *IEEE Trans. Power Electron.*, vol. 31, no. 4, pp. 2890–2904, Apr. 2016.
[29] S. Patra, S. Madichetty, and M. Basu, "Development of a smart energy community by coupling neighbouring community microgrids for enhanced power sharing using customised droop control," *Energies*, vol. 14, no. 17, p. 5383, Aug. 2021.
[30] J. Sun, "Impedance-based stability criterion for grid-connected inverters," *IEEE Trans. Power Electron.*, vol. 26, no. 11, pp. 3075–3078, Nov. 2011.
[31] Y. Han *et al.*, "Modeling and stability analysis of LCL-type grid-connected inverters: A Comprehensive overview," *IEEE Access*, vol. 7, pp. 114975–115001, 2019.
[32] F. Shahnia, "Stability and eigenanalysis of a sustainable remote area microgrid with a transforming structure," *Sustain. Energy, Grids Netw.*, vol. 8, pp. 37–50, Dec. 2016.

Sandipan Patra (Member, IEEE) received the B.Tech. degree in electronics and instrumentation engineering from the West Bengal University of Technology, Kolkata, India, in 2011, the master's degree in electrical engineering with specialization in power electronics and application specific integrated circuit (ASIC) design from the Motilal Nehru National Institute of Technology (MNNIT), Allahabad, India, in 2013, and the Ph.D. degree in electrical engineering from the Technological University Dublin, Dublin, Ireland, in 2021.

In 2021, he worked as a Post-Doctoral Researcher at Trinity College Dublin, Dublin. Currently, he is working as a Researcher with the International Energy Research Centre (IERC), Tyndall National Institute, Cork, Ireland. His research interests include low voltage power electronics, community microgrid, HVDC, power quality, and signal processing applications in power electronics.

Malabika Basu (Member, IEEE) received the B.E. and M.E. degrees in electrical engineering from the Bengal Engineering College, Kolkata, India, in 1995 and 1997, respectively, and the Ph.D. degree in electrical engineering from the Indian Institute of Technology, Kanpur, India, in 2003.

From 2001 to 2003, she was a Lecturer with Jadavpur University, Kolkata, India. From 2003 to 2006, she was an Arnold F. Graves Post-Doctoral Fellow with the Dublin Institute of Technology (now TU Dublin), Dublin, Ireland, where she has been a Lecturer since 2006 and a Senior Lecturer since 2016. She has authored or coauthored more than 105 technical publications in various international journals and conference proceedings. Her current research interests include grid integration of renewable energy sources, power quality conditioners, and power quality control and analysis; photovoltaics (PVs) and wind energy conversion; HVdc systems; smart grid; and microgrids.